

quency, one can envision the use of higher frequencies from which massive economies could be realized. Readily available variable-frequency a-c power would free our society from the limitations imposed by confinement to 60-Hz power. A prime example is the possibility of replacing the standard 60-Hz motor with one capable of operating at 100, 500, or perhaps 1000 Hz or more. At these higher frequencies, an electric motor is physically much smaller than a 60-Hz motor of comparable horsepower rating. The output horsepower of a motor is proportional to the product of speed and torque. Holding torque constant, the horsepower increases with higher-frequency (and therefore high-speed) operation. At present, high-frequency motors are used only for special-purpose applications, such as in aircraft, where there is a clear incentive to minimize both size and weight. A 25-horsepower, 400-Hz motor weighs roughly 30 pounds, whereas the 25-horsepower counterpart at 60 Hz weighs nearly 500 pounds. With ACS technology, it will ultimately be possible to replace large industrial motor installations with comparatively small but equally effective high-frequency units.

The costs of producing, installing, maintaining, and replacing such motors will be dramatically lower than today's costs. The same arguments apply to driven equipment such as pumps and compressors.

Tomorrow's Opportunities

Other applications of ACS technology are yet to be explored. The same technology used to produce an ACS variable-speed device might also be used to produce power processing units of other types, including power converters and inverters for use on electric utility power transmission networks. Such devices might lower the cost of integrating high-voltage d-c systems into a-c networks and allow the many technical advantages of d-c power transmission to be more fully exploited (8). Other device applications might increase power transmission system reliability, lower network operating costs, and reduce land usage for transmission line rights-of-way.

Future applications could also include systems for integrating the power outputs from solar photovoltaic panels, fuel

cells, windmills, and battery systems into conventional power networks. We therefore expect that power processing by semiconductor devices will be a technology of major, broad significance in the not-too-distant future.

References and Notes

1. Arthur D. Little, Inc., *Energy Efficiency and Electric Motors* (Publication PB-259 129; National Technical Information Service, Springfield, Va., 1976).
2. Industrial motor usage is reviewed in *Integral Horsepower Motors and Associated Controls* (Frost & Sullivan, Inc., New York, 1978).
3. R. L. Jacschke, *Controlling Power Transmission Systems* (Penton/IPC, Cleveland, 1978).
4. H. W. Weiss, paper presented at the 19th Annual Petroleum and Chemical Industry Conference, New York, 1972.
5. J. Guyeska, paper presented at the 22nd Annual Petroleum and Chemical Industry Conference, New York, 1975.
6. J. G. Anderson, *Variable Frequency Inverter for AC Drives* (Technical Association of the Pulp and Paper Industry, Atlanta, Ga., 1977).
7. Based on internal forecasts by Exxon Company USA.
8. N. Hingorani, *EPRI (Electr. Power Res. Inst.) J.* 3, 6 (June 1978).
9. The authors wish to acknowledge Richard H. Baker's conceptualization efforts and inventiveness originally at the Massachusetts Institute of Technology in developing the alternating-current synthesizer technology now being pursued by Exxon Corporation. We also wish to acknowledge the project development leadership provided by R. L. Ricci, venture manager of the ACS group, and the assistance provided in preparing this article by T. J. Fossland, L. H. Levenberg, and especially T. P. Schiano of the ACS planning group.

Effect of Cosmic Rays on Computer Memories

J. F. Ziegler and W. A. Lanford

Almost everyone who has had extended experience with electronic computers has witnessed unexplained events in which a single digit of a number appears to change spontaneously, or perhaps the computer itself suddenly stops, and no way can be found for it to repeat the failure. Within the computer industry these problems are known as "soft fails," which differentiates them from the "hard

fail" of a bad electronic circuit that must be replaced. A soft fail in a computer memory may be defined as the spontaneous flipping of a single binary bit, which when later tested will prove to be operating correctly.

The appearance of soft fails in computers has recently become prominent because of the α -particle problem (1-3). This problem was suddenly recognized in 1978 after a new generation of electronics with very small circuit components was introduced. Alpha particles (helium nuclei) are the decay particles of radioactive chains of atoms which start

with uranium or thorium atoms and have emission energies between 5 and 10 million electron volts. They are produced by traces of uranium or thorium in or near the electronic circuits. These α -particles can produce up to 3 million electron-hole pairs (but not more) within the silicon crystal on which the electronic circuits are fabricated. Until 1978 electronic components in computers were apparently not sensitive to noise bursts of 3 million electrons, so the problem was not recognized earlier.

To understand the magnitude of the problem, one must realize the incredible reliability of electronic circuits and the almost immeasurably small amounts of uranium or thorium that can cause problems. Typically, engineers define integrated circuit reliability in units of chip fails per million hours, with nominal reliability rates of one fail per megahour. Note that this is chip fails, not individual component fails, and a chip may contain 64,000 bits of memory. This means that the mean time-to-fail of each bit on the chip is 7,500,000 years. However, in a large computer there may be 1000 such chips, which means that a soft fail might occur once very 1000 hours (\approx 6 weeks).

J. F. Ziegler is manager of ion beam techniques at IBM-Research, Yorktown Heights, New York 10598. W. A. Lanford was with the Wright Nuclear Structure Laboratory at Yale University, New Haven, Connecticut, and is currently at the State University of New York, Albany 12203.

Various authors (2, 3) have estimated that this fail rate can occur with uranium or thorium concentrations below 1 part per million.

The discovery of soft fails produced by α -particles leads directly to the question of the effects produced by cosmic rays. Ultimately, to produce a computer error, the cosmic ray must interact within the silicon crystal and produce a mov-

sider several typical circuit components and calculate the probability for soft fails induced by the cosmic flux. The effects of building shielding (such as ceilings and walls) and of diminished shielding (as in airplane computers at an altitude of 10,000 meters) are then estimated. (A schematic summary of cosmic-ray-induced errors is shown in Figs. 12 and 13.)

Summary. A method is developed for evaluating the effects of cosmic rays on computer memories and is applied to some typical memory devices. The sea-level flux of cosmic-ray particles is reviewed and the interaction of each type of particle with silicon is estimated, with emphasis on processes that produce bursts of charge. These charge pulses are then related to typical computer large-scale integrated circuit components and cosmic-ray-induced errors are estimated. The effects of shielding (such as building ceilings and walls), altitude, and solar cycle are estimated. Cosmic-ray nucleons and muons can cause errors in current memories at a level of marginal significance, and there may be a very significant effect in the next generation of computer memory circuitry. Error rates increase rapidly with altitude, which may be used for testing to make electronic devices less sensitive to cosmic rays.

ing charged particle that generates a burst of electron-hole pairs of sufficient quantity and density to affect electronic circuit components.

Our purpose in this article is to develop a method for predicting the number of cosmic-ray-induced soft fails in electronic circuit components. To do this we examine quantitatively all significant particle-solid interactions that can produce moving charged particles, evaluate the electronic noise burst these particles produce, and relate these bursts to the sensitivity of typical electronic circuit components. Our calculations of cosmic-ray-induced memory errors do not imply probable computer performance, since it is possible to detect and correct errors with system design. We first review the incident flux of cosmic-ray particles at sea level. We consider each type of particle and analyze how it interacts with silicon, producing either a wake of charge or other particles which then produce bursts of charge. Then an estimate is made of how much of the charge from each interaction can reach the electronic circuits on the silicon surface. We con-

Pickel and Blandford (4) have studied the effects of cosmic rays on memory devices in satellites. They pointed out that without the shielding provided by the earth's atmosphere, orbiting memory devices were exposed to a sufficient flux of very high energy heavy-ion cosmic rays to explain the observed soft-fail rate (4). These results are not directly relevant to the problem of soft fails at sea level, where the flux of heavy-ion cosmic rays is essentially zero. However, some of their device modeling is similar to that presented here and hence provides some confirmation of that aspect of our treatment of the sea-level problem. An earlier brief study of this problem was also given by Wallmark and Marcus (5).

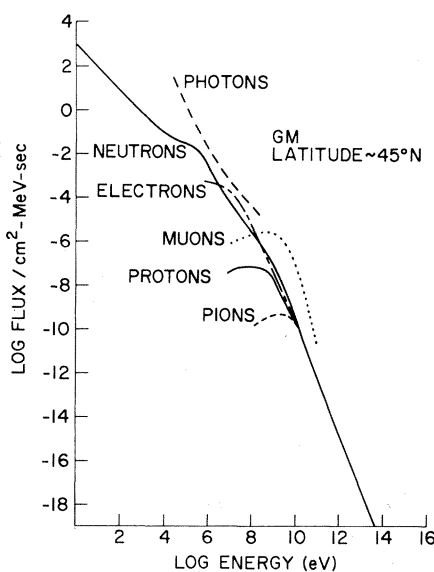


Fig. 1. Flux of cosmic-ray particles at sea level. The curves are average values and large fluctuations exist that are attributed to magnetic latitude, time of day, season, solar cycle, angle of incidence, and so on. Geomagnetic (GM) latitude 45°N was chosen because of the availability of extensive experimental data. The magnitude of these curves changes rapidly with altitude (see Fig. 10). The muon flux is for μ^- particles; the total muon flux ($\mu^- + \mu^+$) is 2.29 times this value.

Cosmic Rays at Sea Level

Primary cosmic rays are galactic particles of very high energy—up to 10^{19} eV. Because of the vast distances of the galaxy, their origin is unknown. A particle of 10^{16} eV makes so many orbits as it penetrates the microgauss field of the galaxy that by the time it reaches the earth no evidence of its origin can be deduced from its trajectory. One consequence is that primary cosmic rays are completely isotropic as they penetrate the earth's atmosphere and interact with the atoms of the atmosphere to cause showers of particles, which we call cosmic rays. These showers were discovered by Hess (6), who found that ionization in a balloon-borne ionization chamber first diminished and then increased rapidly as the chamber rose in the atmosphere. This result is now explained by the process of three or more steps that determines the flux of particles reaching the earth's surface.

The initial particles, the primaries, have a flux of about 1600 per square meter per second, a mean energy of ~ 7 GeV, and an energy (E) spectrum that falls off at the rate of $E^{-5/2}$. (Particles with energies below ~ 1 GeV are deflected by the earth's magnetic field and do not cause showers.) The incident ions are protons, helium ions, and heavier ions, each having about one-third of the total energy. Because of their very high energies, even the heavy ions interact like individual nucleons, and we can consider the incident flux to be 87 percent protons and 13 percent neutrons. Almost all of the primaries effectively disappear by altitudes of 20,000 m.

The secondary particles, produced by interaction of the primaries with the gas atoms of the atmosphere, include nucleons, mesons, electrons, and photons. The secondaries either slow down and are stopped within the atmosphere (particularly the electrons and protons), produce further cascades of particles, or spontaneously decay into other particles. This absorption and conversion process is quite complex.

Finally, the remnants of the cascade strike the earth. Experimental values are available for the flux and energy distribution of the photons, electrons, protons, neutrons, muons, and pions and are shown in Fig. 1. Our sources for these data are primarily (7-11). There are many large variations in the measured fluxes, due to effects attributed to magnetic latitude, time of day, season, solar cycle, and so on, but these have been averaged in Fig. 1. We have also averaged

overall angles of incidence, using azimuthal flux curves where they are available. At sea level, high-energy particles ($> 10^9$ eV) are mostly incident within a solid angle of about 1 radian, while lower energy particles are more nearly isotropic because they result from many cascades. (The orientation of computer electronic devices relative to the vertical will be discussed.)

Interactions That Produce

Bursts of Charge

Only certain types of particle interactions with silicon semiconductors produce electronic bursts that can affect electronic circuits. We are dealing with circuit components with dimensions of the order of micrometers and a time sensitivity of less than 1 second (various devices are sensitive in time from 10^{-9} to 10^{-1} second). From Fig. 1, only very low energy neutrons and photons have flux intensities such that two particles might be coincident on a device, and these will be shown to be of negligible importance. In an extensive single shower other coincidences might occur. We consider here only the effects of isolated particles penetrating the silicon chip.

Since we are concerned with computer binary information, we consider electronic devices that mainly flip or latch into one of two possible states. Therefore for any transient electronic noise to have an effect it must be larger than some threshold value, called the device's critical charge, Q_{crit} . For example, the most sensitive present computer memory component appears to be a charge-coupled device, which stores small amounts of charge in isolated potential wells with a very high packing density. Typical charges may be about 50,000 electrons per bit (12). This is about a factor of 10 lower than the minimum charge in an electronic transistor circuit. We assumed that a sudden spontaneous 20 percent variation in charge may cause the device to invert, which gives $Q_{\text{crit}} = 10^4$ electrons.

A second factor is the volume over which the charge is spread. To cause an error, the threshold charge must be absorbed by a single device. The circuit structures may be considered to be a two-dimensional array of thin films with active areas of $\sim 100 \mu\text{m}^2$. However, they will produce space-charge regions that may penetrate several micrometers into the silicon, and within these volumes almost all charge will be collected. Further, the diffusion length of electrons

in silicon is typically greater than the crystal thickness, so approximately half the charge deposited in the entire silicon volume will end up diluted on the surface with the electronic circuits. The amount of charge a single device will collect from a deep event falls off geometrically with the distance from the event. Considerations of the device dimensions, the space-charge regions, and the probability of diffusion lead to useful effective dimensions (mean collection diameter and volume) in which Q_{crit} must be deposited for a soft fail to occur.

For the general reader, this article has been written so that it is possible to skip the details of evaluating the electromagnetic, nuclear, and weak interactions of particles with silicon and to go either to the section on the sensitivity of computer components to bursts of charge for discussions of electronic components and circuits, or to the section on the variation of error rate with altitude and shielding for a summary of the magnitude of these effects.

Charged Particle Interactions with Silicon

We first consider the physics of electromagnetic interactions of charged particles with silicon. All types of energetic charged particles have two basic types of interactions with silicon, producing ionization wakes along the path of the particle and recoiling silicon nuclei from close collisions.

Ionization effects. Energy loss of particles in silicon has been extensively studied because of the use of silicon semiconductors for particle detectors. Ionization wakes produced by electrons, protons, and muons will be about the same at the same particle velocity. The energy they lose to electronic processes goes into both collective effects such as plasmons (oscillations of the electron gas) and binary effects such as the creation of energetic electrons. Theoretical analysis of the formation of electron-hole pairs is very complex because one must consider the details of the band gap and the curvature of the band edges. Experimentally, however, the problem is simple; the formation of electron-hole pairs is relatively independent of the particle velocity (over the velocity range of interest here) and takes a constant fraction of the energy loss to the target electrons. The number of pairs formed is found by dividing this by the pseudo-generation energy of 3.6 eV per pair (13). Heavy ions are more complex than energetic protons or electrons because they

are partially shielded by their own electrons (and the shielding is velocity-dependent) and they lose significant energy to the target nuclei (such energy loss is negligible in electron and proton stopping). It is beyond the scope of this article to describe the detailed analysis of the energy loss of particles to electronic processes.

We have established the important values of energy loss from both fundamental theory and experimental data (14-16), and Figs. 2 and 3 show the final results, based mainly on (16). In Fig. 2 we give the line density of electron-hole pairs created per unit path length for muons, electrons, protons, helium ions, and silicon ions in a silicon target. The spatial distribution of these carriers about the particle track is not well known, but it can be assumed that they occur primarily within $0.1 \mu\text{m}$ of the path. For the case of silicon ions there will be a reduction of the net available electron-hole pairs due to recombination, the actual rate of which depends on the electric field at the path and the resulting rate at which the carriers are swept apart. We have assumed no recombination in our later calculations.

Figure 3 shows the total electron-hole pairs generated for each type of particle as a function of particle energy. It differs from the distribution that would be obtained by merely integrating the curves of Fig. 2 because energy losses are included that do not generate electron-hole pairs (14). This difference is significant only for heavy ions such as silicon.

Escape of long-range α -particles. The interaction of cosmic rays with silicon often produces α -particles, which can cause noise bursts that definitely can lead to soft fails. It will be convenient to simplify the analysis of α -particle-produced ionization wakes. As shown in Fig. 2, the electron-hole production rate of helium particles peaks at about 0.5 MeV, with a drop-off by a factor of 4 at 10 MeV and of 8 at 20 MeV. Alpha particles emitted in nuclear reactions can have high energies and can travel long distances in silicon; for example, a 10-MeV α -particle has a range of $70 \mu\text{m}$ (15). Therefore many particles emitted from deep in the silicon may have their maximum energy loss near the electronic circuits on the surface of the semiconductor, and alphas produced near the surface may pass out of the silicon, doing no damage.

We have developed a simple model that allows an estimate of the number of alphas that have their maximum ionization wake in a region near the surface.

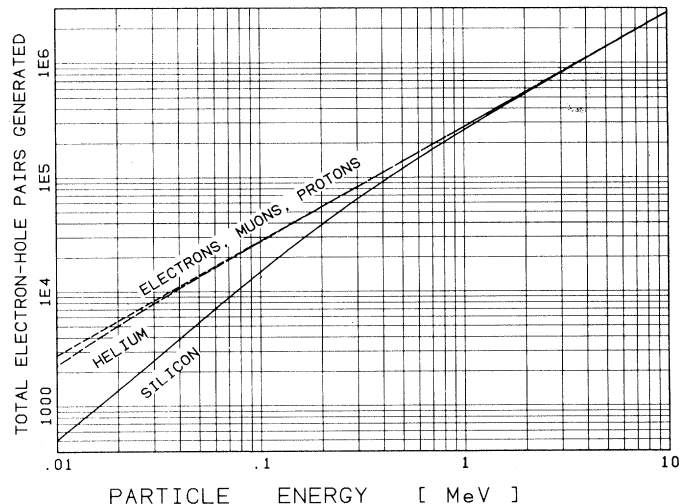
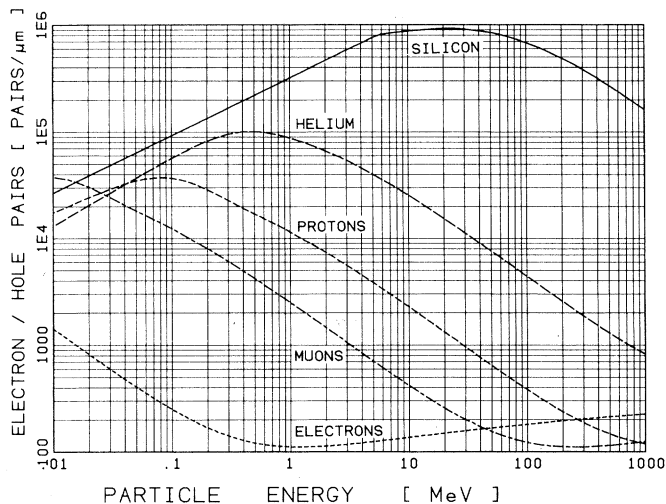


Fig. 2 (left). Ionization wake density of electron-hole pairs in silicon following the passage of various charge particles. An electron-hole pair is created for about every 3.6 eV of energy lost to target electrons by each particle. This process is surprisingly independent of particle velocity and is well verified experimentally, but not theoretically. No experiments have evaluated the lateral distribution of these charges about the particle trajectory, but it is assumed most are within a Debye length of the particle track ($< 0.1 \mu\text{m}$). No density-effect corrections have been made for the relativistic electrons. Fig. 3 (right). Total electron-hole pair creation by particles in silicon. Energy loss of the particles to target nuclei is assumed not to create electron-hole pairs (16, 49).

We assume that the alphas are monoenergetic, isotropic, and produced uniformly throughout the silicon. If the range of the alphas from their creation point to their ionization peak is R , we wish to determine the number N of alphas per unit area that will peak within a distance D of the silicon surface, which we assume is the collection depth for the circuits. We evaluate this for the two cases where $R \geq D$ and $R \leq D$ by determining the portion of the surface of a sphere of radius R that lies within a distance D of the surface. We find

$$N = \rho_\alpha \left(D - \frac{R}{4} \right) \quad (R \leq D) \quad (1)$$

$$N = \rho_\alpha \left(\frac{D}{2} + \frac{D^2}{4R} \right) \quad (R \geq D) \quad (2)$$

assuming a uniform production rate ρ_α of alphas per unit volume. The value of R for helium ions in silicon (15) is

$$R = \exp \left[\sum_{i=0}^5 a_i (\ln E)^i \right] - 2 \quad (3)$$

where R is in micrometers, E is the initial alpha energy in kiloelectron volts, and the coefficients $a_i = -4.1621, 0.98241, 0.10621, -0.058012, 0.0074353,$ and -0.00026865 for $i = 1$ to 5, respectively. The 2 in Eq. 3 is the range of a 0.5-MeV alpha and is subtracted from the total range (in brackets) to give the range of the peak of the electron-hole distribution (Eq. 3 is valid up to 10 MeV).

This first-order analysis of α -particle wakes does not consider the fact that for very sensitive components, the ionization wake within the device of high-energy α -particles passing completely

through the device may reach levels of Q_{crit} . Our knowledge of the α -particle energy distribution is incomplete so we use the simplified model above, noting that this may significantly underestimate the error rate of sensitive components.

Coulomb-induced recoils. The second common electromagnetic interaction between particles and silicon produces recoiling energetic heavy ions. Whenever the fast charged particles scatter from the silicon atoms, the silicon nuclei recoil. For electrons and muons the recoil energy can be approximated by using the formalism of the relativistic Coulomb scattering of point charges. The differential scattering cross section for two point charges is called the Mott-Rutherford cross section and may be expressed (17, 18) as

$$\frac{d\sigma}{d\theta} = \pi \cos \left(\frac{\theta}{2} \right) \text{cosec}^3 \left(\frac{\theta}{2} \right) \times \left[\frac{Z_1 Z_2 e^2 (M_1 + M_2)}{M_1 M_2 v^2} \right]^2 f(\beta) \quad (4)$$

with

$$f(\beta) = (1 - \beta) \left\{ 1 - \beta^2 \sin^2 \left(\frac{\theta}{2} \right) + \pi \alpha \beta \sin \left(\frac{\theta}{2} \right) \left[1 - \sin \left(\frac{\theta}{2} \right) \right] \right\}$$

$$\beta = v/c$$

$$\alpha = Z_2/137$$

where $d\sigma/d\theta$ is the differential cross section for scattering into the center of mass angle θ of a projectile with atomic number Z_1 and mass M_1 , a relativistic velocity v , and energy E , on a target atom of

Z_2 and M_2 . Also, e is the charge on an electron and c is the velocity of light.

We wish to determine the cross section σ_{Th} for obtaining a recoiling silicon atom with an energy above some minimum threshold value E_{min} . This can be done by integrating Eq. 4 over those angles which result in recoiling silicon nuclei with energies greater than E_{min}

$$\sigma_{\text{Th}} = \pi \left(\frac{Z_1 Z_2 e^2 (M_1 + M_2)}{M_1 M_2 c^2 \beta^2 \gamma} \right)^2 \times (E' - 1 - \beta^2 \ln E' + \pi \alpha \beta \{ 2 [(E')^{1/2} - 1] - \ln E' \}) \quad (5)$$

where

$$\gamma = (1 - \beta^2)^{-1/2} = 1 + \frac{E}{M_1 c^2}$$

$$E' = \frac{2E}{M_2 c^2 E_{\text{min}}} (E + 2 M_1 c^2)$$

with E' the ratio of the maximum possible energy transfer to the specified threshold energy.

Equation 5 will be used later to calculate generation rates for electronic noise pulses from recoiling silicon atoms. Because nuclei are not point charges there are serious limitations to using this formula, but the results will be compared to available data. In general, Eq. 5 yields cross sections that are too large, and since these interactions are usually not the primary sources of noise pulses, we use Eq. 5 mainly to indicate the magnitude of various recoil processes. Once the cross section for producing recoiling silicons is established, we can evaluate the electron-hole pairs generated by this moving heavy atom, using Figs. 2 and 3.

Rates of Induced Bursts of Charge

We now evaluate the individual particle interactions with silicon quantitatively and produce "burst-generation" curves, which allow the calculation of computer memory errors for many types of computer devices. The burst-generation curves are in the form of either charge per path length, as for the ionization wake of a particle, or charge per unit volume, for silicon recoils.

The final computer error rates (or chip rates) will be found from

Error rate =

$$A \sum_i D C \int_{E_1}^{E_2} B F S dE \quad (6)$$

where A is the active area of the planar devices in the computer (or in the chip). We sum over all possible particle interactions i , multiplying the appropriate device dimension D (mean diameter for the linear processes of Fig. 2 and active volume for the volume processes) by the collection efficiency C of that volume, the integral of the burst-generation curves B , the appropriate particle flux F of Fig. 1, and the shielding S of the particle flux by building structures, and we integrate over all energies of particle i . If the device has both depletion volumes and drift collection volumes (as discussed in the following section) a suitable average volume is used for the volume-dependent processes.

In producing the burst-generation curves we made some simplifications. Primarily, we assumed that light particles emitted in nuclear reactions have a range R much greater than the device active volume depth D for the evaluation of Eqs. 1 and 2, and conversely that heavy recoil particles have $D \gg R$. Typically,

the light particles have a mean energy of ~ 5 MeV and a mean range of $25 \mu\text{m}$ in silicon, and the heavy particles have an energy of 0.2 MeV and a range of $\sim 0.2 \mu\text{m}$. For devices with active volume dimensions near these two limits, it would be necessary to do the detailed calculation that we outline for each of our B curves specifically for the device in question. We describe below the calculation of the B curves for each particle-silicon interaction; the interactions are numbered I-1, I-2, and so on.

Electron Interactions with Silicon

Electrons interact with silicon (I-1) by producing a wake of electron-hole pairs as shown in Figs. 2 and 3, and (I-2) by elastically scattering and producing recoiling silicon nuclei. They also produce charged particles from Coulomb excitation of the silicon nucleus, but this effect has a small cross section and is unimportant. No permanent damage due to a single electron can be seen in any of the electrical characteristics of silicon (19).

Elastic scattering of electrons from silicon has been studied experimentally in detail. In general, the cross section calculated from Eq. 4 is at least 20 times greater than the experimental values for electron energies of 250 and 500 MeV (20). However, there is also significant inelastic scattering to levels of a few million electron volts in silicon, which somewhat reduces the overestimate of silicon recoils. We use Eq. 5 to generate Fig. 4, which shows the electron-induced silicon recoils above various threshold energies for a unit volume of silicon. We will show that this interaction is not a significant effect in producing computer errors, so a detailed evaluation of the

scattering cross section (21) is not necessary. The silicon recoil burst-generation curve from electron scattering is found by interpolating Fig. 5.

Proton Interactions with Silicon

Protons interact with silicon (I-3) by producing an ionization wake of electron-hole pairs, (I-4) by scattering and producing heavy nucleus recoils, and (I-5) by producing α -particles from nuclear reactions. The electron-hole pair production (I-3) is shown in Figs. 2 and 3.

Proton-induced silicon recoils (I-4). The evaluation of the number of recoiling silicon nuclei above some energy, E_{min} , produced by scattering protons must include both electromagnetic and nuclear interactions. To incorporate these effects, the differential cross section for proton elastic scattering at low energies was calculated, using the optical model of nuclear scattering (22, 23). At high energies (billions of electron volts) this model cannot be relied on, and we used experimentally determined angular distributions of 1-GeV protons (24). For our purposes, the important result is that the proton elastic scattering angular distributions vary only slightly from target to target, and we extrapolated the results of these experiments to deduce the angular distributions for silicon recoils from elastically scattered protons. Figure 5 shows the burst-generation curves for the production of silicon recoils with energies greater than E_{min} . These curves combine the energy and angle dependence of the proton elastic scattering in a convenient form for calculating failure rates for particular devices. It is perhaps worth noting that, in appropriate units, B is simply the cross section for producing silicon recoils with energy greater than E_{min} times the atomic density of silicon ($5 \times 10^{10} \mu\text{m}^{-3}$).

Alpha particles produced by protons on silicon (I-5). The nuclear reaction $\text{Si} + p \rightarrow \alpha + \dots$, where p is a proton, has been studied experimentally in detail (25, 26). The cross-section threshold occurs at about 9 MeV, and at 40 MeV the reaction has a cross section of 0.22 barn (10^{-28}m^2). Especially applicable to our problem are the results of Walton *et al.* (26), who put a beam of protons through a thin silicon sample, then melted the silicon and measured the released helium with a mass spectrometer. Since helium does not diffuse in silicon at room temperature, this clever experiment measures all alpha generation over all possible exit channels of the reaction. The

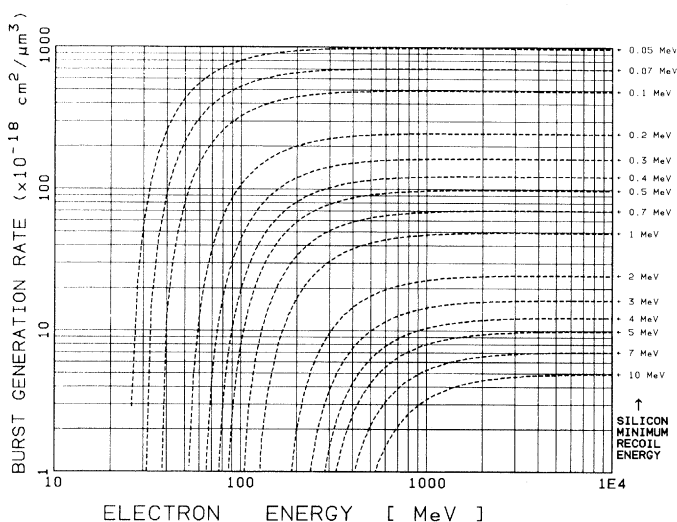


Fig. 4. Generation of energetic silicon recoils from scattering of high-energy electrons. Each curve is the integral of recoils above the minimum silicon recoil energy noted on the right ordinate. These curves are simply derived (based on the Mott-Rutherford formula) and are believed to be the upper limit of the number of silicon recoils.

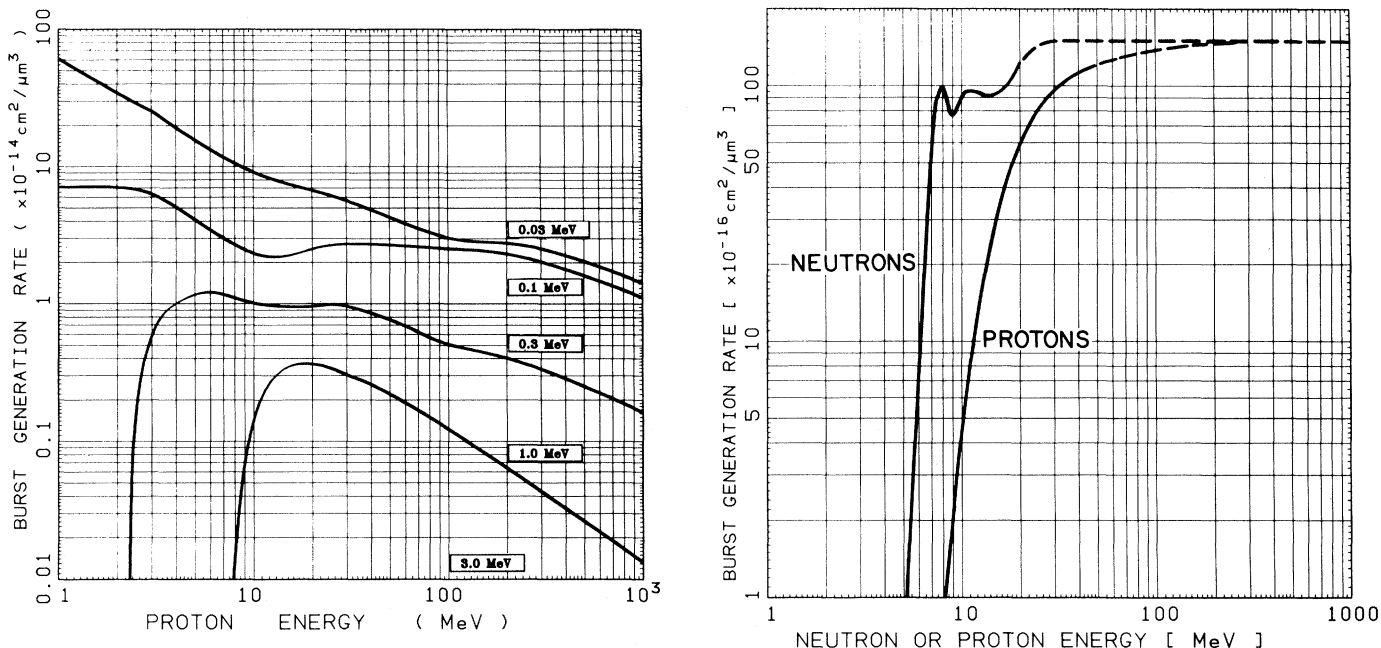


Fig. 5 (left). Generation of energetic silicon recoils from scattering of protons. Each curve is the integral of recoils above the minimum silicon recoil energy indicated on the plot. These curves are from optical model calculations which include both electromagnetic and nuclear interactions (see text). Fig. 6 (right). Burst-generation of protons and neutrons incident on silicon and producing α -particles from nuclear reactions. For the stopping of α -particles near the silicon surface, use half the value of the plotted curve (half the α -particles escape the sample). Since the interaction involves significant contributions from incident particles with energies above 50 MeV, which are strongly anisotropic with a dominant vertical flux, the α -particles will have an anisotropy in the vertical direction and electronic device sensitivity may depend on chip orientation.

cross section of Walton *et al.* for the production of α -particles reaches 0.22 barn for a proton energy of 40 MeV, in good agreement with other results (25). We use the cross sections of this reaction times the silicon atomic density to find the solid-line part of the curves of Fig. 6.

The α -particles emitted in nuclear reactions must penetrate a Coulomb barrier of about 6 MeV. Hence all the α -particles from nuclear reactions with silicon have a range in silicon, R , much greater than the device thickness, D . Some will escape the device without causing errors. To take this effect into account, we use Eq. 2, assuming $R \gg D$, and find that the charge burst-generation curve is half the reaction rate (half the alphas escape from the sample). No account is taken of the layers covering the silicon, which may also produce α -particles that can affect the device.

The high-energy part of the curves of Fig. 6 (dashed line) was determined from general considerations of the interaction of high-energy nucleons with nuclei. The asymptotic value $B = 1.5 \times 10^{-14}$ cm²/μm³ was derived from the assumption that at high energy the total $p + \text{Si}$ cross section was 0.3 barn, which is essentially the measured total absorption cross section (27), and that in these violent collisions with energies of several hundred million electron volts one or more α -particles, or other energetic

heavier particles, will probably be emitted.

Although we have been unable to find any data on the cross section for α -particle production by very high energy protons on silicon, this cross section has been measured for 5.5-GeV protons on silver and uranium (28). For both these targets, the number of α -particles produced corresponds to a cross section of essentially twice the geometric cross section. This large cross section results from the production of two or more alphas in a single collision. A second observation is that at these very high energies, most of the α -particles have energies near the Coulomb barrier. We expect the probability of multiple α -particle emission to decrease with target mass; and therefore assume that the α -particle cross section for protons in silicon is essentially the geometric cross section (this assumption may be a primary source of inaccuracy). Recently, single soft fails in 16K dynamic random access memories have been observed during irradiation by 33-MeV protons (29).

Neutron Interactions with Silicon

More than 100 papers have been published on the interaction of neutrons with silicon. This is due to interest in the re-

sponses of military electronic circuits to nuclear explosions and the effects of intense neutron fluxes from reactors. These papers concern permanent damage to semiconductor devices due to large doses of neutrons (minimum doses considered are about 10¹¹ neutrons per square centimeter). Extrapolation of these results to the effects of one neutron, which we are interested in, would indicate no permanent damage at the level that can be sensed by transistors. [The physical processes involved are discussed in (30) and recent references are compiled in (31).]

Because of the technological importance of neutron-induced reactions on silicon, the existing experimental measurements have been carefully evaluated and the microscopic cross sections for neutrons with energies from 0 to 20 MeV have been calculated. We used this Evaluated Nuclear Data File (ENDF) (22) to predict the ionization burst in silicon from low-energy (≤ 20 MeV) cosmic-ray neutrons and used the theoretical formalism established by the low-energy data to extrapolate to higher energies (21). In some cases these extrapolations can be confirmed by comparison with measured proton-induced reactions on silicon, which, because of the charge symmetry of the nuclear force, should be almost the same as neutron-induced reactions at very high energies.

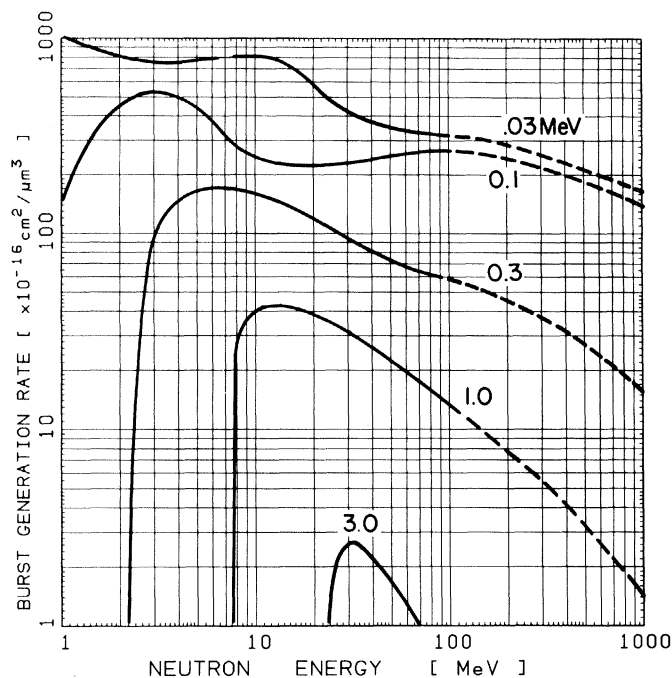


Fig. 7. Burst-generation curves for the nuclear reaction $\text{Si} + n \rightarrow \text{heavy nucleus (recoiling)} + \dots$, where we sum over all significant nuclear reactions. When multiplied by the cosmic neutron flux, the curves give the burst-generation density in silicon for energetic recoils above the indicated minimum energies.

In our analysis of all possible reactions between neutrons and silicon that produce ionization bursts, two are of primary importance. One (I-6) is the creation of energetic silicon nuclei recoiling from the elastic or inelastic scattering of cosmic-ray neutrons. The second (I-7) is the nuclear reaction between neutrons and silicon-producing α -particles.

Neutron-induced silicon recoils (I-6): Shown in Fig. 7 are burst-generation curves for the production of silicon recoils with energies greater than or equal to some minimum energy E_{\min} . The burst-generation function combines the energy and angle dependence of the neutron elastic and inelastic scattering cross section, and it is calculated in the same way as B for proton-induced silicon recoils. The total reaction cross section is evaluated by integrating the differential cross section for elastic and inelastic neutron scattering over angles that result in recoiling silicon atoms with energy above E_{\min} .

The curves in Fig. 7 are based on the evaluated cross-section data from ENDF for $E \leq 20$ MeV. For higher energies, neutron elastic and total reaction cross sections were calculated from an optical model. We included only recoils induced by neutron elastic and inelastic scattering to the first excited state of ^{28}Si and to the continuum and ignored recoils for other reactions such as those producing charged particle emission. This was done because at low energies the elastic and inelastic scattering constitute most of the total cross section. At 20 MeV and above, the most important reactions not

included involve multiple particle emission, for which it is difficult to estimate the spectrum of recoiling heavy nuclei. However, even at these high energies the recoils are dominated by elastic scattering. Hence Fig. 7 gives a reasonable lower limit for the number of silicon recoil counts; a more complete evaluation might increase B by 20 percent for high-energy neutrons. In view of the lack of data for cross sections at high energy, such a correction does not seem justified.

Alpha particles produced by neutrons in silicon (I-7): The threshold for producing α -particles by bombarding silicon nuclei with neutrons (n) is 2.65 MeV. At low energies the important reaction is $\text{Si} + n \rightarrow \alpha + \text{Mg}$, with a cross section that rises to 0.2 barn at 8 MeV and then decreases rapidly above 15 MeV (22, 32-36). Then $\text{Si} + n \rightarrow \alpha + n + \text{Mg}$ becomes important, having a cross section of 0.24 barn at 20 MeV (20). The solid part of the neutron curve in Fig. 6 results from the sum of these two reactions. At energies above 20 MeV, most of the α -particles come from reactions in which other particles (protons or neutrons) are emitted in addition to the α -particle. This part of the curve was evaluated by consideration of the total absorption cross section, as discussed for protons. (It is assumed that above 200 MeV the proton and neutron cross sections are identical.)

As in the case of proton-induced α -particles there is an important geometric effect for neutron-induced alphas (Eqs. 1 and 2). Taking into account the α -particles that escape the silicon before slow-

ing down to their maximum ionization energy, the effective number of maximum ionizing α -particles is a factor of 2 less than the bulk production rate.

Muon Interactions with Silicon

Primary cosmic rays interact with oxygen or nitrogen atoms in the earth's upper atmosphere and both π and K mesons are produced. If these particles do not subsequently interact, their lifetime is less than their transit time to sea level and they spontaneously decay and are the source of muons. Since the primary cosmic rays are 87 percent protons, the ratio of μ^+ to μ^- is not unity but 1.29. Muons are produced at a mean altitude of 15 km. They have a high probability of reaching the earth's surface without producing further cascades, and typically they only leave an ionization wake in the atmosphere (losing about 2 GeV of energy).

A significant aspect of muon flux is geomagnetic latitude. Near the geomagnetic equator there is an increase in magnetic rigidity, and fewer low-energy primary particles penetrate the atmosphere. The number of muons that are produced and reach sea level increases by a factor of 2 to 3 (depending on muon energy) in going from 0° to 50° geomagnetic latitude (37-40) and by a factor of more than 10 at the magnetic poles. The muon electromagnetic interaction with the atmosphere can produce further variations (up to 20 percent), depending on air pressure, temperature, humidity, magnetic storms (the Forbush effect), and time of day (the diurnal effect). We selected the muon flux at 40°N geomagnetic latitude for our calculations.

There are three primary interactions of muons with silicon. Interaction I-8 is the muon ionization wake (Fig. 2), which produces a line of low-density electron-hole pairs. Interaction I-9 is electromagnetic scattering, which produces energetic silicon atom recoils. Finally, interaction I-10 is the complex capture of muons by nuclei, which releases 106 MeV of energy.

The intensity of the ionization wake of muons in silicon peaks at 10 keV (Fig. 2). At this low energy the flux of muons is $2.5 \times 10^{-8} \text{ cm}^{-2} \text{ MeV}^{-1} \text{ sec}^{-1}$, as shown below.

The silicon recoils are initiated by the scattering of very energetic muons. We used Eq. 5 to evaluate the number of silicon recoils produced above various minimum recoil energies, and Fig. 8 shows curves of the integrated recoils as a func-

tion of muon energy. When one of these curves is multiplied by the muon flux, such as that in Fig. 1, the result is the recoils per unit volume above a selected energy threshold value. Examples of this are shown explicitly in the section on calculation of computer errors.

The muon capture interaction involves transmutation of some of the muon mass into energy. First, we need to evaluate how many muons come to rest in silicon. This has been measured (41-45) and calculated (46-48) and reasonable agreement is found (± 20 percent). At a geomagnetic latitude of 40° the sea-level stopping of negative muons is $6.3 \times 10^{-6} \text{ g}^{-1} \text{ sec}^{-1}$ for rock (mean atomic number, 12.8) and $5.6 \times 10^{-6} \text{ g}^{-1} \text{ sec}^{-1}$ for air (mean atomic number, 7.43). Extrapolating to silicon (atomic number, 14), we obtain $7 \times 10^{-6} \text{ g}^{-1} \text{ sec}^{-1} = 1.6 \times 10^{-5} \text{ cm}^{-3} \text{ sec}^{-1} = 5.8 \times 10^{-8} \mu\text{m}^{-3}$ per 10^6 hours.

By combining this stopping rate with a calculation of muon range, we can estimate the flux of muons with energies of 0 to 10 keV needed to evaluate the wake ionization effects of these very slow muons. We calculated the range of muons by using the energy loss rates given in Fig. 2 and the transport equation expansion of Littmark and Ziegler (49) and found that 10-keV muons have a range of 70 nanometers. Hence, the low-energy muon ($\mu^- + \mu^+$) flux = $(2.29) \times (1.6 \times 10^{-5} \text{ cm}^{-3} \text{ sec}^{-1}) \times (70 \times 10^{-7} \text{ cm}) / (0.01 \text{ MeV}) = 2.5 \times 10^{-8} \text{ cm}^{-2} \text{ sec}^{-1} \text{ MeV}^{-1}$. As seen in Fig. 1, this flux is consistent with an extrapolation of the higher energy flux data.

Most integrated circuits are being fab-

ricated on silicon crystals about $400 \mu\text{m}$ thick. Range calculations show that 3-MeV muons have a range of $400 \mu\text{m}$, and therefore the integrated circuit chip will stop all muons with energies of 0 to 3 MeV. These stopping rates are for negative muons only. The positive muons will not be significant because they decay into an electron and two neutrinos with negligible electronic effect.

The negative muons that stop in silicon may either decay into electrons and neutrinos (28 percent) or be captured into an atomic orbit in a silicon atom (72 percent) (50, 51). Since a negative muon is not an electron, it is not kept in an outer orbit by the Pauli exclusion principle and it quickly cascades down into a $1s$ orbit. Since the muon is 200 times heavier than an electron, its $1s$ orbit is largely within the nucleus. It has a high probability of combining with a proton through the weak interaction: $\mu^- + p \rightarrow n + \nu + 106 \text{ MeV}$. If the muon and proton were at rest, the neutron would have 5.7 MeV of energy and the neutrino (ν) would carry off $\sim 100 \text{ MeV}$. The actual energy released varies with the momentum of the capturing proton in the silicon nucleus and a much larger energy than 5.7 MeV is available. This "internal conversion" process may involve complex three-body kinematics between a neutrino, a heavy recoiling nucleus, and any emitted nucleons. We analyze this reaction by assuming that after the emission of the neutrino there is a stationary highly excited nucleus. Many de-excitation branches are possible, but the only ones that are important are those that produce charged particles or create an energetic

recoiling residual nucleus. Of the muons that are captured, 28 percent result in no particles being emitted, 15 percent result in charged particle emission, 67 percent result in neutron emission, with 10 percent emission of both charged particles and neutrons (52-60).

We first consider the charged-particle emission. The 15 percent are ~ 10 percent protons, 5 percent deuterons, and < 1 percent tritons or α -particles [there may be several percent alphas (58, 60)]. The shape of the energy spectrum of the charged particles may be described by an exponential with decay constant, λ ,

$$N(E) \sim \exp(-E/\lambda) \quad (7)$$

where $N(E)$ is the number with energy E and λ for proton emission is about 4.6 MeV. This expression is valid only above the minimum proton energy of 1.4 MeV. The fraction of total protons $N(\mu^-, p)$ with energies above the threshold energy E_{\min} is

$$N(\mu^-, p) = 1.356 \exp(-E_{\min}/4.6) \quad (8)$$

The number of magnesium recoils can be similarly determined by assuming only single-particle emission and conservation of momentum. If E_{Mg} is the minimum Mg recoil energy to be considered, the fraction with energy greater than E_{Mg} is

$$N(\mu^-, \text{Mg}) = 1.356 \exp(-27E_{\text{Mg}}/4.6) \quad (9)$$

with $E_{\text{Mg}} \geq 0.052 \text{ MeV}$.

Similarly, we can evaluate the emitted decay neutrons and the associated recoiling ^{27}Al nuclei. The neutrons also peak at a few million electron volts and their energy spectrum is exponential

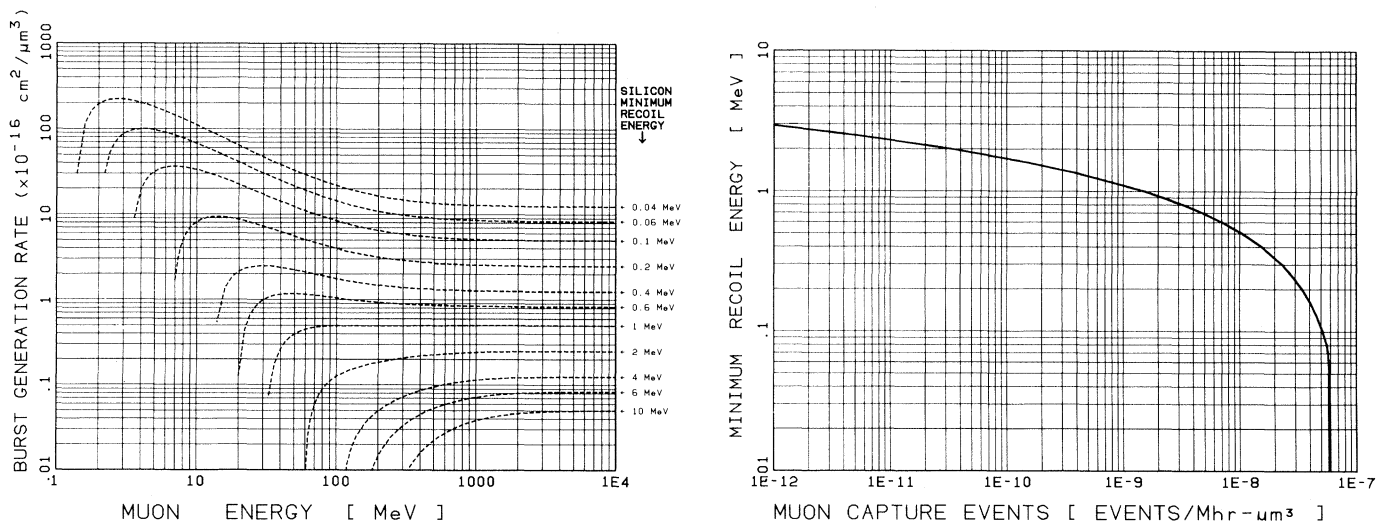


Fig. 8 (left). Electromagnetic scattering of incident muons producing energetic silicon recoils. Each curve shows the integrated recoils above the minimum recoil energy noted on the right ordinate. The calculation is based on relativistic scattering of two point charges. Fig. 9 (right). Generation rate of energetic nuclear recoils following the capture of muons by silicon. The muon capture rate slightly increases with concrete shielding at a rate of 10 percent per meter of concrete.

Table 1. Typical electronic device parameters. These component dimensions are believed to be typical for proposed computer memory circuits. They do not represent any commercial product. Similar components are discussed in (2, 12, 61).

Parameter	d-RAM (64K)	CCD (64K)	CCD (256K)
Active area, μm^{2*}	100	200	80
Stored charge, e^-	1,500,000	180,000	50,000
Critical charge, Q_{crit}, e^-	300,000	36,000	10,000
Depletion depth, μm	3	6.5	3
Mean collection diameter, μm	12	16	11
Mean collection volume, μm^3	800	2,700	600
Bits per chip	65,536	65,536	262,144

*Area refers only to a single-bit-cell capacitor and excludes other susceptible capacitors such as those in the bit lines and the sense amplifiers. Circuit duty cycle is assumed to be unity.

with $\lambda \sim 7.1$ MeV, so the fraction of total neutrons with energies above a threshold energy will be

$$N(\mu^-, n) = 1.325 \exp(-E_{\text{min}}/7.1) \quad (10)$$

with the corresponding ^{27}Al recoils being

$$N(\mu^-, \text{Al}) = 1.325 \exp(-27 E_{\text{min}}/7.1) \quad (11)$$

where we assume simple two-body breakup with a minimum neutron energy of 2 MeV and a minimum recoil of 0.074 MeV.

We combine the recoiling heavy nuclei described by the sum of Eqs. 9 and 11 to produce the burst-generation curve for muon capture in silicon (Fig. 9). As we will show later, this curve is usually independent of shielding.

To summarize the interactions of muons with silicon, the ionization wake (I-8) is found by using the generation curves of Fig. 2. The silicon recoil (I-9) generation curve is found by obtaining the minimum silicon recoil energy in Fig. 3, then interpolating in Fig. 8 for the proper curve. Muon capture (I-10) produces recoiling heavy nuclei with simultaneous emission of neutrons, protons, and deuterons. This generation rate is

found by using Fig. 3 to find the minimum silicon recoil corresponding to the device, Q_{crit} , and then finding the generation rate in Fig. 9. We ignore the lightly ionizing particles that are emitted, but these are described by Eq. 8 and their ionization tracks are described in Fig. 2.

Sensitivity of Computer Components

We selected two types of components from the vast array of computer devices to illustrate the calculation of the potential sensitivity of computer devices to cosmic rays. These components are charge-coupled devices (CCD's), proposed for very large medium-speed memories, and dynamic random access memories (d-RAM's), used for very large high-speed memories. A third type of device, the bipolar transistor, should also be considered, but its analysis is too complex for this article. Although we discuss devices described in the literature, we use them only to obtain typical electrical characteristics; our calculated sensitivities do not include important aspects of the total circuitry, such as duty cycle and cycle time, which may mitigate the predicted effects.

Table 2. Chip errors induced by sea-level cosmic rays. These error rates are based on several simplifying circuit assumptions; actual performance will vary with component design and circuit operation.

Interaction	Chip error rate (events per 10^6 hours)		
	d-RAM (64K)	CCD (64K)	CCD (256K)
(I-1) e^- ionization wake	0	0	0
(I-2) $e^- \rightarrow \text{Si}$ recoils (EM)*	0	< 1	< 1
(I-3) p^+ ionization wake	0	140	1300
(I-4) $p^+ + \text{Si} \rightarrow \text{HN}$ recoils†	< 1	< 1	< 1
(I-5) $p^+ + \text{Si} \rightarrow \text{He}$	< 1	< 1	< 1
(I-6) $n + \text{Si} \rightarrow \text{HN}$ recoils	1	100	250
(I-7) $n + \text{Si} \rightarrow \text{He}$	6	22	20
(I-8) Muon ionization wake	0	330	1700
(I-9) Muon \rightarrow silicon recoils (EM)*	< 1	3	4
(I-10) μ^- capture \rightarrow HN recoils†	< 1	7	8
Total	~ 7	~ 600	~ 3000

**"Si recoils (EM)" indicates close electromagnetic (EM) collisions that induce energetic recoiling silicon nuclei. †"HN recoils" indicates a summation over all recoiling heavy nuclei (HN) from the nuclear reaction indicated.

The CCD stores small amounts of charge in potential wells at the interface of a silicon crystal and a covering insulator such as SiO_2 . The charge migrates in a track ("racetrack") so that a long string of sequential bits can be read consecutively. Once in the racetrack the charge that represents a bit is not refreshed (it is called floating charge), and during its transit of the course it is vulnerable to charge bursts. This device is believed to have the smallest amount of charge per bit of any current commercial device and one 64K-bit array (12) has bit cell sizes of 12 by 14 μm , with a total of 180,000 electrons for a 1; for a 256K-bit device the charge would be of the order of 50,000 electrons per bit (2).

The d-RAM is produced commercially on a large scale. In one device of this type the 0 or 1 of a stored bit is the presence or absence of charge on a small capacitor, which is merely a thin-film conductor, a very thin oxide, and the silicon substrate. The sense of the capacitor is detected by a highly sensitive amplifier. In one current design (61) the bit is fabricated with an area of 170 μm^2 with a capacitance of 50 femtofarads, and it writes into this cell with 5 volts. This means that the stored charge is 1.5×10^6 electrons.

Both types of memories are transient, since the charge stored in a bit is slowly neutralized due to leakage in the silicon from the bulk and the periphery of the cell. These devices are therefore cycled, and every few milliseconds each cell is interrogated and then refreshed with a full charge; this is why they are called dynamic memories. While a cell is being refreshed it may not be sensitive to charge bursts, but it cannot be used as active memory. We have assumed a 100 percent active state for all devices for simplicity, but chip reliability will be improved by any reduction in this floating state.

The sensitivity of both CCD's and d-RAM's to bursts of charge has been shown by experiments in which they are subjected to α -particles from radioactive sources (2, 3). The CCD devices are much more sensitive because of their lower stored charge. The effect of a single α -particle may be visualized by considering a CCD memory of all 1's; a track of 0's is spontaneously induced outlining the ionization wake of the α -particle (62).

We assume that the sensitivity of these devices to cosmic rays may be deduced from the relative magnitude of two parameters, the critical threshold charge of the device and the burst of charge that

migrates to the device from a cosmic-ray interaction in silicon. This latter process involves two regions, the depletion depth of the device, in which 100 percent of the induced charge is collected, and the volume outside this, in which the induced charge must diffuse with only part entering the device.

Diffusion of a line of charge in silicon has been studied in detail by Kirkpatrick (63) in his analysis of the effects of α -particles on electronic circuits. He assumes that the charge initiates along a line, the recombination is negligible, the diffusivity of charges is $25 \text{ cm}^2/\text{sec}$, and the surface is a perfect charge sink. He arrives at several important rules about the collection efficiency for lines of charge. The most useful to us is that for a burst of charge below the device, there is significant collection of the charge down to depths that subtend a solid angle of approximately 1 steradian. This angle refers to the complete space charge cross section, because full collection of all charge that drifts into this electric field is assumed. Therefore, the effective collection diameter of the devices we consider will be 50 percent greater than the space charge diameter.

Kirkpatrick also pointed out to us that if a detailed calculation were made of the diffusion of charge from deep bursts, the effective collection depth would not be a constant but would depend on the size of the charge burst. Distant charge bursts may cause errors if the burst is far larger than Q_{crit} .

Calculation of Circuit Error Rates

We can now calculate the sensitivity of the devices to cosmic rays. These devices typically have the characteristics shown in Table 1 (2, 12, 61). In this section we assume an unshielded sea-level flux of cosmic rays (Fig. 1) and use the steps outlined above to evaluate each type of particle-silicon interaction. We then use Eq. 6 to find the final error rate, which is shown in Table 2.

In Table 1, the depletion depth is found from the device voltage, silicon type, and silicon resistivity. The mean collection diameter is found by constructing a cell with its depletion depth plus 50 percent, which approximates the distance of charge diffusion from beyond the depletion zone. The cell is constructed in three dimensions, and we average over all incident directions to obtain the mean diameter (taking into account that some particles will only clip corners). The mean collection volume is

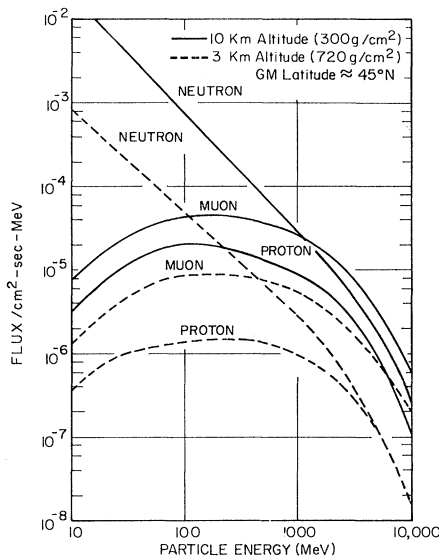


Fig. 10. Experimentally determined cosmic-ray fluxes at altitudes of 3 and 10 km at about geomagnetic latitude 45°N . Similar curves for electrons could not be found, so their interaction with silicon was omitted in the calculations of computer errors at various altitudes.

the volume of the cell. The chip area and the active area are estimated from data in (2, 12, 61).

In Table 2, the direct-ionization interactions (I-1, I-3, and I-8) are calculated by a three-step process. First, we determine Q_{crit} per micrometer for the three devices by dividing Q_{crit} by the mean collection diameter, and we obtain 25,000, 2,250, and 910 e^- per micrometer. We then use Fig. 2 and obtain the energy range E_1 to E_2 for which electrons, protons, and muons will generate more than this charge density. For example, for protons in the d-RAM we would obtain $E_1 = 0.02$ and $E_2 = 0.25$ MeV. Finally, we evaluate the total number of electron-hole pairs between these two energies to determine whether it is larger than Q_{crit} . For these two energies we find 5,000 and 90,000 total pairs in Fig. 3. Subtracting these, we have 85,000 pairs produced between E_1 and E_2 , which is less than the Q_{crit} of the d-RAM, so the protons are incapable of creating errors in the d-RAM at any energy. A similar analysis of protons for the CCD 64K device gives $E_1 = 0$ and $E_2 = 10$ MeV, for a total of 2.8×10^6 electron-hole pairs, which makes this particle capable of causing a soft fail. With these energy limits, we now integrate Eq. 6 over the corresponding particle flux in Fig. 1 (Fig. 1 shows the μ^- flux and the total muon flux is 2.3 times this value). It is necessary to draw in the low-energy charged particle flux curves in Fig. 1 because there seem to be no experimental data for protons and

electrons and we assume a constant slope from the lowest experimental points. We finally multiply this integral by the chip active area.

The direct electromagnetic interactions causing silicon recoils (Table 2, I-2 and I-9) are calculated by determining the minimum silicon recoil energy corresponding to Q_{crit} , then interpolating in Fig. 4 or Fig 8 for the burst-generation curve, multiplying this by the flux from Fig. 1, integrating over all particle energies, and finally multiplying by the device mean collection volume and number of bits per chip.

The failure rate due to neutron-induced heavy nucleus recoils (Table 2, I-6) is calculated from Eq. 6 and Fig. 7. For the short-range highly ionizing silicon recoil events, the minimum recoil energy, corresponding to Q_{crit} , is found from Fig. 3, and then the burst-generation function appropriate to this E_{min} is found by interpolating in Fig. 7. The B is then multiplied by the neutron flux (Fig. 1) and integrated over all neutron energies ($E_1 = 0$ and $E_2 = \infty$). Finally, this integral is multiplied by the active volume of the device and the number of devices per chip.

The failure rate due to α -particles from $n + \text{Si}$ reactions (I-7) is calculated in the same way, using the correct B from Fig. 7. There is one important difference because of the fact that the α -particles typically have ranges that are large compared to the thickness of the device. From Eq. 2 (with $R \geq D$), this effectively halves the number of fails for thin devices, so one calculates the fail rate by using Eq. 6 and B from Fig. 7 and multiplies by 0.5.

The proton nuclear reaction processes (Table 2, I-4 and I-5) are calculated similarly to the neutron ones, by finding the minimum recoil energy corresponding to Q_{crit} of the device (Fig. 3), then using Figs. 5 and 6 for the two burst-generation curves, multiplying this by the proton flux (Fig. 1), integrating this product over all proton energies, and finally multiplying by the device charge collection volume and the number of devices per chip.

The muon capture interaction (I-10) is evaluated by finding the burst-generation value from Fig. 9 and multiplying this by the device collection volume and the number of devices per chip from Table 1.

For the total error rate, we sum the respective columns. It should be noted that we have analyzed only one component of our three representative circuits, and Table 1 is only a partial indication of expected error rates.

Variation of Error Rate with Altitude and Shielding

There will be important variations of error rates with different cosmic-ray fluxes, such as those associated with changes in geomagnetic latitude, solar flares, altitude, and shielding. Altitude variation will be important because of the opportunity it provides for accelerated testing of device sensitivity to cosmic rays. Shielding by concrete walls and ceilings will be a factor in test variations in different locations.

We chose to calculate error rates at altitudes of 3 and 10 km because of the availability of detailed cosmic-ray flux data there. The primary fluxes are shown in Fig. 10 (except for electrons, for which we could find no data) and we used the procedures of the previous section. We found large changes in the total error rates from 3 to 10 km, with all interactions increasing. If these calculations were continued to higher altitudes, we would expect the muon effects to peak at about 15 km and then diminish as muon production from decaying mesons is reduced. Then the proton interactions would probably dominate the error rates because of the large proton/neutron ratio. Finally, in space we are subject primarily to ionization wake effects from the solar wind (64).

For the effects of shielding we consider only concrete; review articles are available for other materials (65, 66). For charged particles the attenuation with

depth in concrete is rapid. We evaluated the change in flux with depth by integrating stopping power curves for muons, protons, and electrons in concrete (16, 49). The problem is more complex for the neutron flux because when high-energy neutrons hit nuclei they produce secondary neutron cascades. However, most secondaries have low energies, except for those produced by primaries with energies above 150 MeV, which is where the cosmic-ray flux falls rapidly. We use the cascade calculations of Patterson and Thomas (66) and Wallace (67) to produce the shielding curves (S in Eq. 6) for neutrons in concrete; our results are shown in Fig. 11. Muon capture events are a special case because of the shape of the flux curve at sea level (Fig. 1). Both experiments (45, 48) and theory (47) show that the muon stopping in rock increases with depth down to several meters, where it is 20 percent higher than at sea level. These altitude and shielding results are summarized in Fig. 12.

All devices are remarkably sensitive to altitude. For example, they would show an increase in the error rate by about a factor of 4 going from Los Angeles to Albuquerque—an altitude increase of ~ 2 km. The CCD's have Q_{crit} levels low enough to be sensitive to muon ionization, so moderate shielding with concrete has no effect. The d-RAM error rate decreases with the thickness of concrete shielding to levels below one error per 10^6 hours.

Variations in Cosmic-Ray Flux

The calculated error rates shown in Fig. 12 are for the average cosmic-ray flux, excluding bursts from solar events. Variations in flux are so large, however, that even circuits with very low error rates may have brief bursts of soft fails. For example, a large solar event on 12 November 1960 produced peak fluxes of energetic particles (> 20 MeV) that were 25,000 times the flux of galactic particles hitting the earth. The types of particles produced by solar events are somewhat different from the galactic flux, but more importantly, the energy distribution in a solar flux is steeper (fewer particles with energies above 1 GeV) than that in the galactic flux. So the sea-level flux from solar events is much smaller than the flux due to galactic particles. For the solar event mentioned above, the flux of neutrons with energies above 20 MeV at sea level may have increased by a factor of about 1.5 to 3 (68) and the error rate of circuits would have increased almost linearly by the same amount. This event was the largest of the 1953 to 1964 solar cycle.

To discuss the general nature of these solar bursts, we define a solar event as one that produces at the earth a proton flux exceeding $0.5 \text{ cm}^{-2} \text{ sec}^{-1} \text{ sr}^{-1}$ with energies above 20 MeV. Although these energy and intensity thresholds are arbitrary, they give a reasonable separation of special high fluxes from normal recurrent events not associated with solar

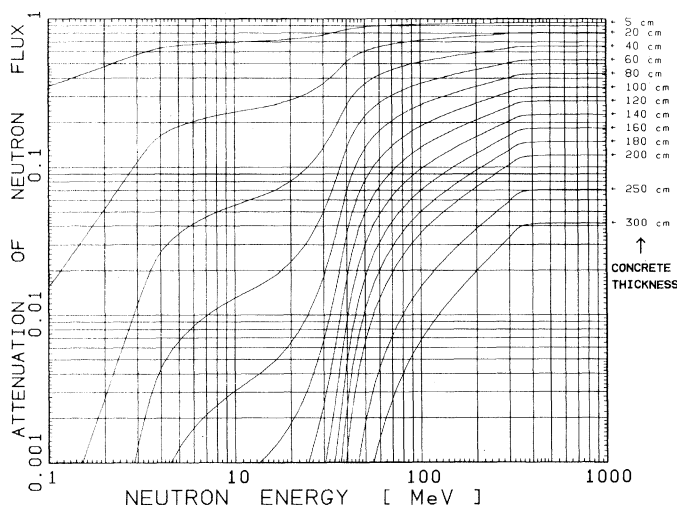
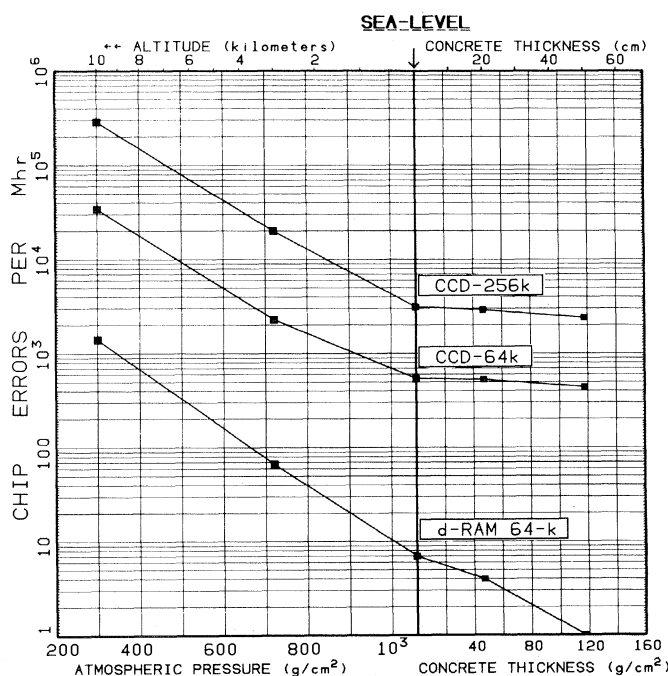


Fig. 11 (left). Reduction of neutron flux with concrete shielding (density, 2.45 g/cm^3). The calculation includes cascade effects that produce secondary neutrons and is based on the work of Wallace (67) and Patterson and Thomas (66). To use this calculation, interpolate for the desired shielding and use this for the shielding term S in Eq. 6. Fig. 12 (right). Summary of cosmic-ray-induced chip errors. These results represent typical calculations; many details of circuit characteristics have been omitted (see text). The CCD error rates decrease only slowly under concrete shielding because the dominant interaction is with low-energy muons, which have an increased flux below concrete. The d-RAM improves under concrete because of the attenuation of the neutron flux. The increase in error rate with altitude offers the possibility of accelerated testing of circuit component sensitivity to cosmic rays.



flares. Solar events occur at the frequency of the solar cycle, which has maxima at 11-year intervals (1958, 1969, 1980, . . .). In quiet periods there may be fewer than three solar bursts per year, and when the sun is active there may be more than 20 per year. Primary particles with energies above 20 MeV of galactic origin have a constant flux of $10^8 \text{ cm}^{-2} \text{ year}^{-1}$, while those of solar origin vary from $10^5 \text{ cm}^{-2} \text{ year}^{-1}$ (quiet sun) to $> 10^{10} \text{ cm}^{-2} \text{ year}^{-1}$ (active sun). Usually, solar particle events can be directly related to solar flares; however, there are some particle flux events with no apparent flares, and many flares occur without significant particle fluxes. Particles with high enough energies to cause flux bursts at sea level generally occur only during the explosive initial phase of the flare (66) and last a few hours. The transit time to the earth is not much longer than the photon transit period since these particles typically have velocities greater than two-tenths the speed of light, so only several minutes separate the first x-rays and the following particles. A typical particle burst lasts less than 1 hour, but the unusually large 1960 event above lasted 4 days for particles with energies above 500 MeV and 10 days for those with energies above 20 MeV (69). Because solar particle events have been observed in detail only for two solar cycles, predictions of event occurrence rates and flux spectra would be very speculative. However, we believe that large solar bursts might produce errors in current computers at high altitudes, even in devices with critical charges of 10^6 electrons, because of the very large increase in flux intensity. The concurrence of solar bursts and soft-fail peaks can now be evaluated about 1 week later by referring to appropriate cosmic flux logs (70).

Cosmic-Ray Considerations in Electronic Device Design

In considering device sensitivity to cosmic rays, it must be recognized that there are steps in the error rate dependence on electronic device critical charge, Q_{crit} . These charge thresholds are directly related to nuclear reaction thresholds and peak ionization wake densities, as shown in Fig. 13. Increasing the Q_{crit} of a device above each threshold significantly decreases its sensitivity to cosmic rays. Our results show that most cosmic-ray particles can become significant, depending on device design and shielding. At high altitudes protons probably dominate; near sea level the neu-

trons and muons become important, unless the device is so sensitive that the electron ionization wakes can cause soft fails; and with thick concrete shielding the muons dominate. The following should be considered in making devices insensitive to these effects.

1) The maximum charge density developed by the ionization wake of protons and muons is 30,000 e^- per micrometer of path length, and devices that are insensitive at this level have low error rates. The effective maximum density for electrons is about 1000 e^- per micrometer, because they cannot sustain a higher generation rate for even 1 μm .

2) The second major threshold is sensitivity to helium particles from nuclear reactions. These particles can generate 70,000 e^- per micrometer over paths of $\sim 7 \mu\text{m}$ at the end of their range, so devices that are insensitive at levels above 500,000 electrons are very insensitive to cosmic rays.

3) The orientation of small devices relative to the vertical probably does not affect error rates. For the low-energy particle interactions, ionization wakes and muon capture, the incident particles will be isotropic above the horizon. For nuclear reactions we must inspect the particle energy that creates the highest error rates. Both proton- and neutron-induced error rates peak for particle energies of 2 to 200 MeV. Such particles will be anisotropic, and most will be incident within solid angles of less than 1 sr about the vertical (7, 8). However, these particles penetrate many centimeters of matter and, to first order, their burst generation depends on the active volume of the device, not on orientation.

4) Orientation will affect long electronic components such as bit lines, which may be 3 by 1000 μm . Long components would be susceptible to the ionization wake of higher energy particles ($> 1 \text{ MeV}$) traveling longitudinally through the device. These particles have trajectories strongly oriented along the vertical, with a cosine distribution function of $\cos^n \theta$, where θ is the angle from the vertical, and n ranges from ~ 2 for muons to ~ 4 for protons. Long devices should be oriented horizontally for minimum susceptibility.

5) Error correcting codes (ECC's) are standard circuits in most large computers. These circuits use extra bits to test memory words for soft fails and correct them if they occur. As devices are made smaller, it may become necessary to use ECC's on smaller computers to ensure reliable operation.

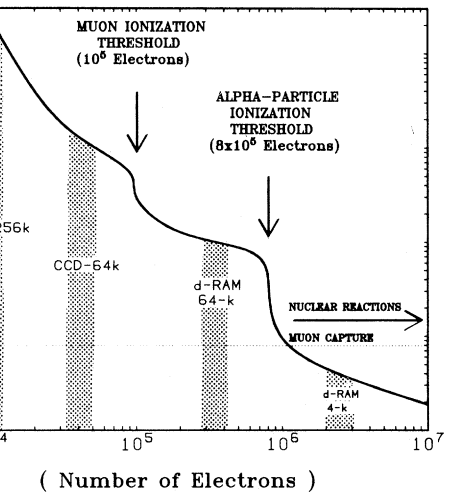


Fig. 13. Estimated error rates for devices similar to those analyzed in the text. Devices were assumed to be about 10 to 15 μm in diameter, operated at 10 volts, and fabricated on silicon of resistivity 10 ohm-cm. Devices with different sizes and voltages may behave very differently. The steps associated with sensitivity to α -particles and muon ionization wakes are shown. If the critical charge for a device drops below one of the thresholds, the error rate may increase 30 times. Before 1978 almost all circuit components had Q_{crit} values above 10^6 electrons, and almost no errors were induced by α -particles from trace amounts of uranium or thorium.

which may be 3 by 1000 μm . Long components would be susceptible to the ionization wake of higher energy particles ($> 1 \text{ MeV}$) traveling longitudinally through the device. These particles have trajectories strongly oriented along the vertical, with a cosine distribution function of $\cos^n \theta$, where θ is the angle from the vertical, and n ranges from ~ 2 for muons to ~ 4 for protons. Long devices should be oriented horizontally for minimum susceptibility.

5) Error correcting codes (ECC's) are standard circuits in most large computers. These circuits use extra bits to test memory words for soft fails and correct them if they occur. As devices are made smaller, it may become necessary to use ECC's on smaller computers to ensure reliable operation.

Conclusions

We evaluated the effects of cosmic rays on three typical computer memory circuits and calculated their probable rates of soft fails. We analyzed only one component of each circuit, and our results may differ from those observed with actual devices because of the effects of duty cycle, operating voltage, silicon resistivity, and so on. The effects we find are marginally significant for current devices such as the 64K d-RAM, but will be important for future electronic circuits. Dramatic increases of soft fails are predicted at airplane altitudes, and this altitude effect can be used to accelerate the testing of devices for sensitivity to cosmic rays. Concrete shielding gives some improvement for special devices, but if the electronics are very sensitive to muon interactions (as are the CCD de-

vices), shielding will not affect error rates.

It is difficult to comment on the accuracy of the calculated error rates because of the unknown accuracy of the many input parameters. There are serious gaps in the fundamental understanding of various interactions. We were unable to find any data on the flux of low-energy (0.001 to 10 MeV) cosmic-ray protons and muons at sea level, and our estimates may be quite inaccurate for the interactions that depend on these fluxes. Few cross sections have been measured for nuclear reactions of 50- to 1000-MeV protons and neutrons on silicon. It is not clear how well nuclear evaporation theory describes the production of (n, α) reactions and the reactions that yield recoiling energetic heavy nuclei. Finally, the critical charge for soft fails in electronic circuits is not usually discussed in published articles and our estimates may be inaccurate.

In spite of these uncertainties, data are available that can be used to put a lower limit on the fail rate induced by neutrons—the dominant mechanism for devices such as the 64K d-RAM. Quenby *et al.* (11) give the number of nuclear disintegrations (stars) induced by cosmic rays (mostly neutrons) in which 40 MeV or more energy is observed in the disintegration fragments. This rate is $1.8 \times 10^{-5} \text{ g}^{-1} \text{ sec}^{-1}$ in air (9, figure 4); and when scaled to silicon this becomes $1.5 \times 10^{-5} \text{ g}^{-1} \text{ sec}^{-1} = 1.2 \times 10^{-7}$ per cubic micrometer per 10^6 hours. This is half the rate calculated for (n, α) reactions (I-7). Thus, star production rates lead us to conclude directly, independent of detailed analyses of cross sections and fluxes, that for devices whose dominant failure mode results from neutron-induced nuclear reactions, the fail rate given in Table 2 is not overestimated by more than a factor of 2.

References and Notes

- S. Hershberger and D. Hanson, *Electron. News* **24**, 1 (28 August 1978); S. Hershberger, *ibid.* **24**, 1 (18 December 1978).
- T. C. May and M. H. Woods, in *Proceedings of the 1978 International Reliability Physics Symposium* (IEEE 78CH 1294-8PHY, Institute of Electrical and Electronics Engineers, New York, 1978), p. 33; *IEEE Trans. Electron Devices* **ED-26**, 1 (1979).
- D. S. Yaney, J. T. Nelson, L. L. Vanskike, *IEEE Trans. Electron Devices* **ED-26**, 10 (1979).
- J. C. Pickel and J. T. Blandford, *IEEE Trans. Nucl. Sci.* **25**, 1166 (1978).
- J. T. Wallmark and S. M. Marcus, *Proc. IRE* **50**, 286 (1962).
- V. F. Hess, *Phys. Z.* **12**, 998 (1911); *ibid.* **13**, 1084 (1912).
- S. Hayakawa, *Cosmic Ray Physics* (Wiley-Interscience, New York, 1969).
- A. W. Wolfendale, Ed., *Cosmic Rays at Ground Level* (Institute of Physics, London, 1973).
- W. M. Lowder and L. R. Solon, "Background radiation—a literature search," *USAEC Rep. NYO-4712* (1958).
- P. Morrison, M. S. Vallarta, K. Sitte, G. Cocconi, G. N. Fowler, A. W. Wolfendale, in *Encyclopedia of Physics* (Springer-Verlag, New York, 1961), vol. 46, No. 1.
- J. J. Quenby, E. Schopper, E. Lohrmann, G. Mauck, D. Lal, B. Peters, in *Encyclopedia of Physics* (Springer-Verlag, New York, 1967), vol. 46, No. 2.
- R. C. Varshney and K. Venkataswaran, *IEEE J. Solid State Circuits* **SC-13**, 681 (1978).
- National Academy of Sciences, *Semiconductor Nuclear-Particle Detectors and Circuits* (Publ. 1593, National Academy of Sciences, Washington, D.C., 1969).
- H. H. Andersen and J. F. Ziegler, *The Stopping and Range of Ions in Matter*, vol. 3, *Hydrogen: Stopping Powers and Ranges in All Elements* (Pergamon, New York, 1977).
- J. F. Ziegler, *The Stopping and Range of Ions in Matter*, vol. 4, *Helium: Stopping Powers and Ranges in All Elements* (Pergamon, New York, 1978).
- , *The Stopping and Range of Ions in Matter*, vol. 5, *Handbook of Stopping Cross-Sections for Energetic Ions in All Elements* (Pergamon, New York), in press.
- N. F. Mott, *Proc. R. Soc. Ser. A* **124**, 425 (1929).
- W. A. McKinley and H. Feshbach, *Phys. Rev.* **74**, 1759 (1948).
- J. C. Corelli, A. R. Frederickson, J. W. Westhead, *IEEE Trans. Nucl. Sci.* **NS-13**, 70 (1966).
- G. C. Li and M. R. Yearian, *Phys. Rev. C* **9**, 1861 (1974) and references cited therein.
- J. F. Ziegler, "The calculation of inelastic electron scattering by nuclei," *USAEC Tech. Publ. 2726E-49* (1967).
- The Evaluated Nuclear Data File is available from the National Nuclear Data Center, Brookhaven National Laboratory, Upton, N.Y.
- D. C. Larson, Oak Ridge National Laboratory, private communication.
- A. Chaumeaux, Division of Nuclear Physics, Saclay, *Annual Progress Report* (1975-1976), p. 227.
- G. Philipp, W.-D. Emmerich, A. Hofmann, G. Kroner, K. Thomas, *Nucl. Phys. A* **160**, 654 (1971); C. E. Moss, C. Detraz, C. S. Zaidius, *ibid.* **170**, 111 (1971); L. M. Colli, G. M. B. Marazzan, R. Bonetti, M. Milazzo, J. W. Smits, *Nuovo Cimento Soc. Ital. Fis. A* **39**, 171 (1977); G. D. Gunn, K. W. Kemper, J. D. Fox, *Nucl. Phys. A* **232**, 176 (1974).
- J. R. Walton, A. Yaniv, D. Heymann, D. Edgerley, M. W. Rowe, *J. Geophys. Res.* **78**, 6428 (1973); *ibid.* **79**, 314 (1974).
- A. Wattenberg, *Handbuch der Physik* (Springer, Berlin, 1957), vol. 40, p. 482.
- A. M. Poskanzer, G. W. Butler, E. K. Hyde, *Phys. Rev. C* **3**, 882 (1971); E. K. Hyde, G. W. Butler, A. M. Poskanzer, *ibid.* **4**, 1759 (1971).
- C. S. Guenzer, E. A. Wolicki, R. G. Allas, R. B. Theus, S. E. Gordon, *IEEE Trans. Nucl. Sci.*, in press.
- E. C. Smith, D. Binder, P. A. Compton, R. I. Wilbur, *ibid.* **NS-13**, 11 (1966).
- W. R. van Antwerp and J. E. Youngblood, *ibid.* **NS-24**, 2521 (1977).
- B. Mainsbridge, T. W. Bonner, T. A. Rabson, *Nucl. Phys.* **48**, 83 (1963).
- R. Potenza, R. Ricamo, A. Rubbino, *ibid.* **41**, 298 (1963).
- P. Jessen, M. Borimann, F. Dreyer, H. Neuert, *Nucl. Data Tables* **A1**, 103 (1965).
- J. K. Dickens, *Phys. Rev. C* **2**, 990 (1970).
- D. Crumpton, *J. Inorg. Nucl. Chem.* **31**, 3727 (1969).
- L. Colli, I. Iori, M. G. Marazzan, M. Milazzo, *Nucl. Phys.* **43**, 529 (1963).
- M. Conversi, *Phys. Rev.* **79**, 749 (1950).
- A. Subramanian, S. Naranan, P. V. Ramana-murthy, A. B. Sahiar, S. Lal, *Nuovo Cimento* **7**, 110 (1958).
- R. M. Tennent, *Prog. Elem. Part. Cosmic Ray Phys.* **5**, 365 (1960).
- E. P. George and J. Evans, *Proc. Phys. Soc. London Sect. A* **63**, 1248 (1950); *ibid.* **68**, 829 (1955).
- S. Kaneko, T. Kubozoe, M. Okazaki, M. Takahata, *J. Phys. Soc. Jpn.* **10**, 600 (1955).
- A. M. Short, *Proc. Phys. Soc. London* **81**, 841 (1963).
- M. Fotino, *Phys. Rev.* **117**, 243 (1960).
- J. C. Barton and M. Slade, in *Proceedings of the 9th International Conference on Cosmic Rays* (Institute of Physics, London, 1965), p. 1006.
- J. Rama and M. Honda, *J. Geophys. Res.* **66**, 3533 (1961).
- J. Takagi and S. Tanaka, *Inst. Nucl. Study Univ. Tokyo Rep. INSJ-110* (1968).
- S. Charalambus, *Nucl. Phys. A* **166**, 145 (1971).
- U. Littmark and J. F. Ziegler, *The Stopping and Ranges of Ions in Matter*, vol. 6, *Handbook of Ranges of Energetic Ions in All Elements* (Pergamon, New York), in press.
- J. C. Sens, R. A. Swanson, V. L. Telegri, D. D. Yovanovitch, *Phys. Rev.* **107**, 1464 (1957); J. C. Sens, *ibid.* **113**, 679 (1959).
- G. G. Bunatyan, V. S. Evseev, L. N. Nikitynk, V. N. Pokrouskii, V. N. Rybakov, I. A. Yutlandov, *Sov. J. Nucl. Phys.* **11**, 444 (1970).
- Yu. G. Budyashov, V. G. Zinov, A. D. Konin, A. I. Mukhin, A. M. Chatrchyan, *Sov. Phys. JETP* **33**, 11 (1971).
- S. E. Sobottka and E. L. Wills, *Phys. Rev. Lett.* **20**, 596 (1968).
- R. M. Sundelin and R. M. Edelstein, *Phys. Rev. C* **7**, 1037 (1973).
- G. H. Miller, M. Eckhause, P. Martin, R. E. Welsh, *ibid.* **6**, 487 (1972).
- R. M. Sundelin, R. M. Edelstein, A. Suzuki, K. Takahashi, *Phys. Rev. Lett.* **20**, 1198 (1968).
- B. MacDonald, J. A. Diaz, S. N. Kaplan, R. V. Pyle, *Phys. Rev. B* **5**, 1253 (1965).
- P. Singer, *Springer Tracts Mod. Phys.* **71**, 39 (1974).
- A. Wyttenbach, P. Baertschi, S. Bajo, J. Hadermann, K. Junker, S. Katcoff, E. A. Hermes, H. S. Pruijs, *Nucl. Phys. A* **294**, 278 (1978).
- L. Vil'gel'mova, V. S. Evseev, L. N. Nikityuk, V. N. Pokrouskii, I. A. Yutlandov, *Sov. J. Nucl. Phys.* **13**, 310 (1971).
- G. R. Rao and J. Hewkin, *Electronics* **5** (No. 20) 109 (28 September 1979).
- E. S. Anolick and L. Chen, in preparation.
- S. Kirkpatrick, *IEEE Trans. Electron. Devices*, in press.
- D. Binder, E. C. Smith, A. B. Holman, *IEEE Trans. Nucl. Sci.* **NS-22**, 2675 (1975).
- S. J. Lindenbaum, *Annu. Rev. Nucl. Sci.* **11**, 213 (1961); A. Rindi and R. H. Thomas, *ibid.* **23**, 315 (1973).
- H. W. Patterson and R. H. Thomas, *Part. Accel.* **2**, 77 (1971); J. Ranft, *ibid.* **3**, 129 (1972).
- R. Wallace, *Nucl. Instrum. Methods* **18**, 405 (1962).
- J. F. Steljes, H. Carmichael, K. G. McCracken, *J. Geophys. Res.* **66**, 1363 (1961). We have corrected the yields shown to separate the neutron flux spike > 10 MeV.
- D. A. Bryant, T. L. Cline, U. D. Desai, F. B. McDonald, *Astrophys. J.* **141**, 478 (1965).
- Preliminary Report and Forecast of Solar Geophysical Data*, a weekly publication of the U.S. Department of Commerce.
- We wish to thank many colleagues who have helped us on this project: J. A. Armstrong, J. E. Baglin, J. P. Biersack, D. A. Bromley, R. W. Keyes, S. Kirkpatrick, D. C. Larson, B. J. Masters, G. A. Peterson, V. L. Rideout, L. M. Terman, and E. A. Wolicki.